Journal of the Mechanics and Physics of Solids 60 (2012) 1122–1136

Contents lists available at SciVerse ScienceDirect

Journal of the Mechanics and Physics of Solids

journal homepage: www.elsevier.com/locate/jmps

On the rheology of dilative granular media: Bridging solid- and fluid-like behavior

José E. Andrade [a,*], Qiushi Chen [a], Phong H. Le [a], Carlos F. Avila [a], T. Matthew Evans [b]

[a] Division of Engineering & Applied Science, California Institute of Technology, Pasadena, CA 91125, USA
[b] Department of Civil, Construction, and Environmental Engineering, North Carolina State University, Raleigh, NC 27695, USA

ARTICLE INFO

Article history:
Received 6 May 2011
Received in revised form
24 February 2012
Accepted 25 February 2012
Available online 3 March 2012

Keywords:
Granular media
Rheology
Rate-dependent
Plasticity
Dilatancy

ABSTRACT

A new rate-dependent plasticity model for dilative granular media is presented, aiming to bridge the seemingly disparate solid- and fluid-like behavioral regimes. Up to date, solid-like behavior is typically tackled with rate-independent plasticity models emanating from Mohr–Coulomb and Critical State plasticity theory. On the other hand, the fluid-like behavior of granular media is typically treated using constitutive theories amenable to viscous flow, e.g., Bingham fluid. In our proposed model, the material strength is composed of a dilation part and a rate-dependent residual strength. The dilatancy strength plays a key role during solid-like behavior but vanishes in the fluid-like regime. The residual strength, which in a classical plasticity model is considered constant and rate-independent, is postulated to evolve with strain rate. The main appeal of the model is its simplicity and its ability to reconcile the classic plasticity and rheology camps. The applicability and capability of the model are demonstrated by numerical simulation of granular flow problems, as well as a classical shear banding problem, where the performance of the continuum model is compared to discrete particle simulations and physical experiment. These results shed much-needed light onto the mechanics and physics of granular media at various shear rates.

1. Introduction

A salient feature of dry granular media is their ability to feature a wide range of complex behavior, even though these materials are composed of relatively simple individual units or particles. Granular matter may behave like a solid in the quasi-static regime, such as a sand dune; or like a fluid when a flow is provoked, such as granular avalanche; or even like a gas when strongly agitated (Jaeger et al., 1996). While the mechanical behavior of granular materials is essentially governed by interactions between particles, the imperfect knowledge of contact forces between particles and prohibitive computational cost renders it impractical to model any field-scale problem by directly utilizing discrete models at the grain scale (Cundall, 2001; Cundall and Strack, 1979). To this end, a continuum description of granular materials is still of great importance for modeling and understanding natural hazards, such as landslides, rock avalanches, and for important industrial applications, such as powder handling, granulates in pharmacy, just to name a few.

Within the scope of interest to this work, the current understandings of granular materials are mostly confined to two extremes, i.e., solid-like behavior and fluid-like behavior. On the one hand, the solid-like state is typically tackled using soil plasticity models emanating from Mohr–Coulomb plasticity theory, see for instance, Andrade and Borja (2006), Andrade

* Corresponding author.
E-mail address: jandrade@caltech.edu (J.E. Andrade).

0022-5096/$ - see front matter © 2012 Elsevier Ltd. All rights reserved.
doi:10.1016/j.jmps.2012.02.011

and Ellison (2008), Manzari and Dafalias (1997), Pestana and Whittle (1999), Schofield and Wroth (1968) among others. These plasticity models have been successfully implemented into numerical tools such as finite element methods and applied to model quasi-static behavior of granular materials see e.g., Andrade and Tu (2009), Desai and Siriwardane (1984), and Tu et al. (2009). Experiments conducted under quasi-static conditions have revealed that the strength of granular materials can be decomposed into a dilatancy strength and a residual strength (Rowe, 1962; Stroud, 1971; Taylor, 1948; Wood, 1990). The dilatancy strength typically vanishes towards the so-called critical state (Schofield and Wroth, 1968; Wood, 1990), where granular materials undergo isochoric deformations. The material strength at the critical state is given by the residual strength, which is considered to be constant and rate-independent.

On the other hand, the flow of granular materials has been a very active research area in the physics community. Much of the work in this area focuses on steady regime of the flows, trying to identify relevant quantities such as flow threshold, kinematic profiles, effective friction. Extensive experiments and discrete particle simulations have been carried out on various configurations and geometries: flow on inclined planes (Berton et al., 2003; Jop et al., 2007; Silbert et al., 2001, 2003), rotating drum (du Pont et al., 2005; Rajchenbach, 1990), plane shear (Thompson and Grest, 1991; Zhang and Campbell, 1992), etc., see also GDR MiDi (2004) for a collection of results, and Delannay et al. (2007) for a review. From a theoretical point of view, even in very simple configurations with sphere-shaped particles, the flow can be very complex to model (du Pont et al., 2005; Silbert et al., 2001). Constitutive models have been developed to capture some of the key features of granular flow. One family of constitutive laws considers local rheology using dimensional analysis, where the effective friction coefficient and volume fraction are expressed as some functions of a dimensionless inertial number I (Jop et al., 2005, 2006; Pouliquen et al., 2006). For instance, in Jop et al. (2006), a flow criteria and the dependence on shear rate were established, analogous to classical viscous Bingham fluids (Fung, 1977). Quantitative predictions for flow shape and velocity profiles have been relatively successful. Still, there are limitations for this approach, such as quasi-static or solid-like regime and hysteresis, which are not correctly captured (Forterre and Pouliquen, 2008). Other approaches have been proposed beyond the local rheology, linking rheology to the evolution of distribution of contacts (da Cruz et al., 2005; Lois et al., 2005), or relating stress tensor to non-local functions of velocity field and material structures (Mills et al., 1999). The depth-averaged or Saint–Venant equations first introduced by Savage and Hutter (1989) have also been successfully applied to capture the main flow characteristics, see, e.g., Greve et al. (1994) and Wieland et al. (1999).

The aforementioned efforts have been mostly focusing on uniform steady flows, and the transition from solid-like to fluid-like state remains an open question in granular materials. This transition is of utmost importance as many applications deal with transient behavior between solid and fluid states. A clear example of this is the recent interest on shear thickening effects in dense suspensions (Brown et al., 2010; Fall et al., 2008). A few efforts in experiments or numerical simulations have been proposed (du Pont et al., 2005; Jop et al., 2007; Orpe and Khakhar, 2004; Zhang and Campbell, 1992), while constitutive models able to bridge these two domains are yet to be developed. One noteworthy model is the one presented in Pailha and Pouliquen (2009), developed for simulating underwater granular avalanches, and where rate-dependence is included via dilatancy and interstitial fluid viscosity. This model can simulate dry granular flows by removing the effect of the fluid viscosity. Aiming at shedding some light into the solid–fluid behavioral transition in granular materials, in this paper we postulate a simple rate-dependent plasticity model. We adopt concepts from critical state soil mechanics (Wood, 1990), where the material strength classically decomposed into a dilatancy strength and a residual strength at critical state. However, unlike the classical critical state models, where the residual strength is constant, rate-dependent residual strength is postulated based on experimental and numerical evidence. Another key ingredient of the proposed model is the role of dilatancy, which is typically neglected in the study granular flows. It is believed that dilatancy plays a key role in the solid-like state, but vanishes in fluid-like state of granular materials. The proposed constitutive model features dilatancy as the main variable controlling solid–fluid behavioral transitions.

The remainder of the paper is structured as follows: in Section 2, the proposed constitutive model is presented within the framework of rate-dependent plasticity. Evolution laws for dilatancy and rate-dependent residual strength are postulated. In Section 3, the model is calibrated and verified using data from a numerical triaxial test done by discrete element simulation. In Section 4, the model is put into tests for simulating a typical granular flow problem and a classical plane strain compression problem in soil mechanics, where results of both classical rate-independent model and the proposed model are compared with experiment data. Finally, some conclusions and discussions are presented in Section 5.

As for notations and symbols used in this paper, bold-faced letters denote tensors and vectors; the symbol '$\cdot$' denotes an inner product of two vectors (e.g. $\boldsymbol{a}\cdot\boldsymbol{b}=a_ib_i$), or a single contraction of adjacent indices of two tensors (e.g. $\boldsymbol{c}\cdot\boldsymbol{d}=c_{ij}d_{jk}$); the symbol ':' denotes an inner product of two second-order tensors (e.g. $\boldsymbol{c}:\boldsymbol{d}=c_{ij}d_{ij}$), or a double contraction of adjacent indices of tensors of rank two and higher (e.g. $\boldsymbol{C}:\boldsymbol{\epsilon}^{\mathrm{e}}=C_{ijkl}\epsilon^{\mathrm{e}}_{kl}$); the symbol '$\otimes$' denotes a juxtaposition, e.g., $(\boldsymbol{a}\otimes\boldsymbol{b})_{ij}=a_ib_j$. Finally, for any symmetric second-order tensors $\boldsymbol{\alpha}$ and $\boldsymbol{\beta}$, $(\boldsymbol{\alpha}\otimes\boldsymbol{\beta})_{ijkl}=\alpha_{ij}\beta_{kl}$, $(\boldsymbol{\alpha}\oplus\boldsymbol{\beta})_{ijkl}=\alpha_{ik}\beta_{jl}$, and $(\boldsymbol{\alpha}\ominus\boldsymbol{\beta})_{ijkl}=\alpha_{il}\beta_{jk}$.

2. Rate-dependent rigid-plastic model for granular media

In this section, we present a rate-dependent phenomenological model to simulate the behavior of granular matter. In particular, the model is founded upon the basic features of material behavior: pressure-dependence, dilatancy, non-associative flow, and strain-rate dependence. The model departs from classic Coulomb plasticity and is able to evolve into Bingham-type flow. Furthermore, the model is cast within the critical state framework (Schofield and Wroth, 1968; Wood, 1990), characterized by a state of isochoric deformations, i.e., zero dilatancy. For simplicity, we describe the model within

the framework of rigid-plasticity and infinitesimal deformations such that $\dot{\boldsymbol{\epsilon}} = \dot{\boldsymbol{\epsilon}}^{\mathrm{e}} + \dot{\boldsymbol{\epsilon}}^{\mathrm{p}}$ applies and $\dot{\boldsymbol{\epsilon}}^{\mathrm{e}} \approx \mathbf{0}$, implying $\dot{\boldsymbol{\epsilon}} \approx \dot{\boldsymbol{\epsilon}}^{\mathrm{p}}$. Adding elastic deformations is standard and will be done in the examples section.

2.1. Yield surface and plastic potential

Consider the two stress invariants of the stress tensor $\boldsymbol{\sigma}$ such that

$$p = \tfrac{1}{3}\operatorname{tr}\boldsymbol{\sigma} \quad \text{and} \quad q = \sqrt{\tfrac{3}{2}}\|\boldsymbol{s}\| \tag{2.1}$$

with $\boldsymbol{s} = \operatorname{dev}\boldsymbol{\sigma}$ as the deviatoric projection of the stress tensor. Frictional materials obey Coulomb-type relationships where, at yielding, the mean normal stress is related to the deviatoric stress via frictional resistance, i.e.,

$$F(p,q) = q + \mu p = 0 \tag{2.2}$$

where μ is typically called the frictional resistance or friction coefficient and is related to the friction angle in granular materials. The frictional resistance can be either assumed constant or a function of the deviatoric strains. Typically, the latter is assumed and a phenomenological model to govern the evolution of μ is postulated.

Now, consider the two invariants of the strain rate tensor $\dot{\boldsymbol{\epsilon}}$, i.e.,

$$\dot{\epsilon}_{\mathrm{v}} = \operatorname{tr}\dot{\boldsymbol{\epsilon}} \quad \text{and} \quad \dot{\epsilon}_{\mathrm{s}} = \sqrt{\tfrac{2}{3}}\|\dot{\boldsymbol{e}}\| \tag{2.3}$$

with $\dot{\boldsymbol{e}} = \operatorname{dev}\dot{\boldsymbol{\epsilon}}$ as the deviatoric projection of the strain rate tensor. In granular materials, Reynolds (1885) first realized the important role of the so-called dilatancy, which effectively couples deviatoric and volumetric components of deformation. This feature distinctly separates granular materials from other materials such as metals, which are non-dilative. It is important to note that dilatancy plays a central role in the mechanical behavior of granular matter. For instance, dilatancy contributes to strength and depending on the relative packing density of the material, it can allow for macroscopic contraction or dilation. Consider the plastic potential

$$Q(p,q) = q + \beta p - c = 0 \tag{2.4}$$

where β is defined as the dilatancy and c is a free parameter to ensure that the stresses in F and Q coincide.

In classic plasticity, the plastic stain rate is obtained from the plastic potential such that

$$\dot{\boldsymbol{\epsilon}} = \dot{\lambda}\frac{\partial Q}{\partial \boldsymbol{\sigma}} = \dot{\lambda}\left(\frac{1}{3}\beta\mathbf{1} + \sqrt{\frac{3}{2}}\hat{\boldsymbol{n}}\right) \tag{2.5}$$

where $\hat{\boldsymbol{n}} := \boldsymbol{s}/\|\boldsymbol{s}\|$ is the unit deviatoric tensor and $\mathbf{1}$ is the second-order identity tensor. From this equation, we can conclude that $\dot{\boldsymbol{e}} := \operatorname{dev}\dot{\boldsymbol{\epsilon}} = \dot{\lambda}\sqrt{3/2}\hat{\boldsymbol{n}}$ and that $\dot{\boldsymbol{e}}$ and $\boldsymbol{s}$ are coaxial. From these realizations it follows that dilatancy is defined such that

$$\dot{\epsilon}_{\mathrm{v}} = \beta\dot{\epsilon}_{\mathrm{s}} \tag{2.6}$$

Note that dilatancy, as the frictional resistance, can be considered either a constant or a function of the deformation. Associative plastic flow would require $\beta = \mu$. Furthermore, a direct constitutive relation is obtained between the deviatoric stress and the deviatoric strain rate, i.e.,

$$\boldsymbol{s} = \eta\dot{\boldsymbol{e}} \quad \text{with} \quad \eta = -\frac{3}{2}\frac{\mu p}{\dot{\epsilon}_{\mathrm{s}}} \tag{2.7}$$

Eq. (2.7) is reminiscent of constitutive relations for non-Newtonian fluids where the deviatoric stress depends on the deviatoric strain rate via a viscosity term η (Fung, 1977; Jop et al., 2006).

The constitutive picture is completed by postulating the evolution of the frictional resistance and dilatancy. We propose a classical stress–dilatancy relation, where the frictional resistance is a function of the dilatancy and some residual resistance such that (Wood, 1990)

$$\mu = \beta + \overline{\mu} \tag{2.8}$$

In classic soil mechanics, $\overline{\mu}$ is the residual resistance of the material and is considered constant. However, flow experiments in granular materials at different deformation rates and at steady-state have shown that the frictional resistance is a function of the deviatoric strain rate (Jop et al., 2006; GDR MiDi, 2004). When at steady-state, the granular material must have mobilized all the dilatancy and must be at critical state so that $\beta = 0$ and $\mu = \overline{\mu}$. Fig. 1 shows typically observed evolution of the residual resistance as a function of the deviatoric strain rate. The figure helps reconcile the apparent rate-independence observed in quasi-static experiments in granular materials: they are conducted at very low shear strain rates. As shear strain rates are increased, the material's residual frictional resistance increases. This phenomenological observation will be a key feature of the proposed model and will afford it capturing solid and fluid features accurately.

Remark 1. As Reynolds (1885) pointed out, it is the dilatancy β that separates granular matter from other materials, say, non-Newtonian fluids. At the same time, pressure p also plays a fundamental role in the mechanical behavior of granular

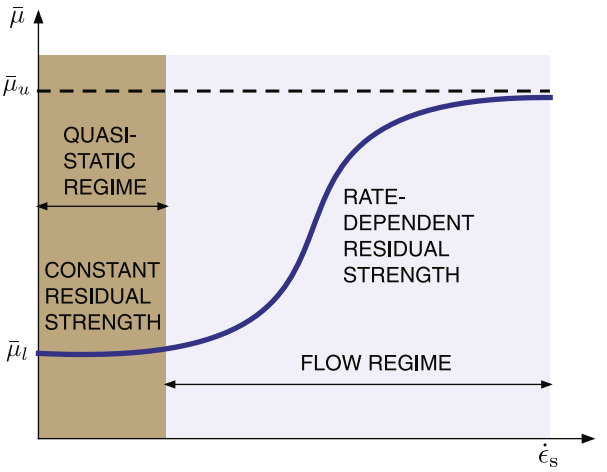

Fig. 1. Observed evolution of the residual frictional resistance in granular material flow at steady-state.

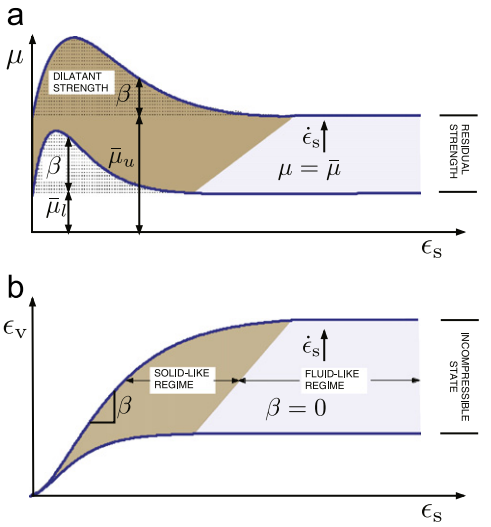

Fig. 2. Interpretation of proposed constitutive model under constant shear strain rates $\dot{\epsilon}_s$ based on axisymmetric compression simulations. (a) Frictional strength μ and (b) volumetric strain ϵ_v vs. shear strain ϵ_s. Both strength μ and dilatancy β (alternatively, ϵ_v) are shown to increase with the increasing shear strain rate $\dot{\epsilon}_s$.

matter. The consequence of dilatancy is that the deviatoric and volumetric strain rate components are coupled (see Eq. (2.6)) and that frictional strength is enhanced by the dilatancy (see Eq. (2.8) and Fig. 2). Once dilatancy is fully spent or critical state is achieved ($\beta = 0$), flow becomes incompressible. At this point, the formulation reduces to pressure-dependent incompressible non-Newtonian flow. As shown in Fig. 2, dilative strength is what separates the solid-like state from the fluid-like state. Consequently, in this model, the critical state marks the transition between solid-like and fluid-like states.

Remark 2. Classical plasticity has considered $\overline{\mu} = \overline{\mu}_l$ constant since, for most applications, quasi-static conditions ($\dot{\epsilon}_s \approx 0$) apply. However, it can be seen from the above constitutive framework that the residual strength $\overline{\mu}$ is rate dependent and can be included in the formulation relatively easily. Numerical experiments under triaxial compression at different strain rates and infinite slope show this important feature in the following sections.

Remark 3. Fig. 2 shows interpretations of the proposed strain-dependent simple model. The figure implies that at $\epsilon_s = 0$ we have $\beta = 0$. This is assumed for simplicity and clarity but it is an approximation as it neglects the initial compression in the material. Adding elastic compressibility would eliminate this approximation. The explicit form of the model should be considered as an approximation; our objective is not to postulate a specific model form or evolution, but rather a combined framework that allows the co-existence of classic frameworks such as critical state and Bingham flow, affording enhanced accuracy.

2.2. Evolution equations

In the present model, the governing material plastic internal variables are the frictional resistance μ and the dilatancy β. As mentioned before, in traditional rate-independent plasticity models (which have dominated in granular materials literature), the residual strength $\overline{\mu}$ is considered constant and, therefore, in order to complete the constitutive picture, it suffices to postulate an evolution law for the dilatancy. Experiments suggest that, at quasi-static rates, the dilatancy might be dependent on pressure and deviatoric shear strain. Therefore, a general form of dilatancy could be written as $\beta = \beta(p,\epsilon_s)$, as has been used to model the dilatancy evolution of granular soils under quasi-static conditions using constant parameters (Borja et al., 2003; Tu et al., 2009). However, for simplicity of presentation—and lack of thorough experiments, we will only consider the deviatoric shear strain dependence, and postulate a simple function for the dilatancy evolution as

$$\beta(\epsilon_s) = \beta^* \frac{\epsilon_s}{\epsilon_s^*} \exp\left(1 - \frac{\epsilon_s}{\epsilon_s^*}\right) \tag{2.9}$$

where β^* is the maximum dilatancy and ϵ_s^* is the corresponding shear strain. It should be noted that the evolution equation for β in Fig. 2 allows for shear rate-dependence, if necessary. In Eq. (2.9) this feature has been turned off. The rate-dependence of dilatancy has not been observed in the numerical experiments conducted herein, but cannot be discarded at this point.

By the same token, numerical and experimental results on steady-state flow of granular materials have shown a clear rate dependence of $\overline{\mu}$, similar to that shown in Fig. 1. The rate dependence for the residual strength can be proposed to take the simple form (Jop et al., 2006)

$$\overline{\mu} = \overline{\mu}_l + \frac{\overline{\mu}_u - \overline{\mu}_l}{1 + \dot{\epsilon}_s^*/\dot{\epsilon}_s} \tag{2.10}$$

where $\overline{\mu}_l$ is the lower bound for the residual resistance when $\dot{\epsilon}_s \to 0$. This is often called the quasi-static range. On the other hand, $\overline{\mu}_u$ is the upper bound achieved as $\dot{\epsilon}_s \to \infty$. The upper bound would mark the end of the flow regime and transition into the gaseous regime (Jaeger et al., 1996) (where this model no longer applies). Furthermore, $\dot{\epsilon}_s^*$ signifies the shear strain rate at which the residual friction $\overline{\mu} = 1/2(\overline{\mu}_l + \overline{\mu}_u)$.

Remark 4. The residual strength form shown above is slightly simpler than that proposed in Jop et al. (2006). The complete expression should depend on the dimensionless quantity I, which is proportional to the shear strain rate $\dot{\epsilon}_s$, but also depends on pressure. However, the effect of pressure has been ignored and the resulting expression above is simpler. Nevertheless, the complete expression depending on I can be implemented if desired. The results presented in this paper show that the simpler evolution of $\overline{\mu}$ is reasonable in this context.

The resulting evolution for the friction resistance can be written as a function of the dilatancy and residual resistance and is given as a function of the cumulative shear strain and the shear strain rate so that

$$\mu(\epsilon_s, \dot{\epsilon}_s) = \beta(\epsilon_s) + \overline{\mu}(\dot{\epsilon}_s) \tag{2.11}$$

This expression is an enhancement of the classic rate-independent plasticity models to account for the rate effects observed in the residual resistance. Also, this framework incorporates basic plasticity axioms for granular materials such as the critical state (Schofield and Wroth, 1968; Wood, 1990). In fact, achievement of the critical state (i.e., $\beta = 0$) signifies the transition into incompressible rate-dependent flow, as we will see in the examples below.

Remark 5. The evolution laws introduced above are by no means complete or universal. They are simply introduced to account for the most salient features of granular matter in the simplest way. As more experiments become available, better calibration of the above evolution laws can be achieved or new evolution laws can be proposed all together. Nevertheless, the next sections will show that this simple framework can capture several important features in the material behavior and the transition between the solid-like and fluid-like states, even though very simple evolution laws have been used.

Remark 6. It is interesting to compare the model presented herein with the model advocated in Pailha and Pouliquen (2009). In the model presented in Pailha and Pouliquen (2009), rate-dependence is introduced by allowing the dilatancy (via the packing fraction) to depend on shear rate. Additionally, rate dependence is built into the model from the viscosity of the interstitial fluid, present in underwater granular avalanches, see Eq. (3.21) in Pailha and Pouliquen (2009). On the other hand, the model presented here, stems from the classic equations of plasticity theory and allows for rate dependence to enter via the residual strength $\overline{\mu}$ and, possibly, dilatancy β. While both models are phenomenological, their efficacy needs to be further verified by extensive validation programs with experiments that can probe the transition between solid-like and fluid-like states in granular deformation.

3. Model calibration and verification

In this section, the model is calibrated using data from numerical experiments performed by discrete element method (DEM) and verified through a series of triaxial compression tests under different loading rates. Of particular interest is that

the model is able to capture desired features of granular materials, which cannot be obtained by using conventional rate-independent plasticity models or granular flow models alone. Also, computational efficiency is demonstrated by implementing the plasticity model within the return mapping framework (Simo and Hughes, 1998).

3.1. Model calibration with discrete element simulation

The numerical experiments used to calibrate the model are performed using DEM. Initial configuration and loading conditions for the DEM simulation are shown in Fig. 3. The sample size is $(48 \times D_{50})^3$, where D_{50} is the mean particle diameter. Lateral confining stresses of 25 kPa are applied and the top of the sample is compressed under strain controlled boundary conditions. Two strain rates are applied: a low rate of 0.002/s and a high rate of 0.04/s. Parameters used in the DEM simulation are summarized in Table 1.

The stress ratio versus shear strain for both low and high strain rate tests are shown in Fig. 4(a). As typically seen in dense granular materials, for both cases, the stress ratio increases to a peak value and then gradually decreases (softening behavior) to a constant value, i.e., the residual resistance $\overline{\mu}$. For high loading rate, $\overline{\mu} = 1.5$ and for low loading rate, $\overline{\mu} = 1.05$.

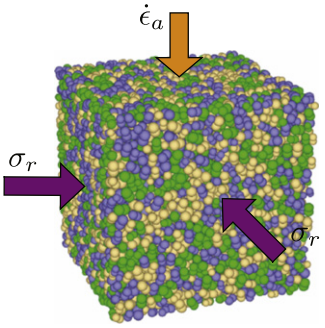

Fig. 3. Initial configuration and loading conditions for polydispersed granular assembly in DEM computation. Different colors correspond to different particle diameters. (For interpretation of the references to color in this figure legend, the reader is referred to the web version of this article.)

Table 1
Parameters used in DEM triaxial simulations for calibrating model.

Symbol	Parameter	Value
N	Number of particles	9092
D_{50}	Mean particle diameter	0.125 m
k_n	Normal contact stiffness	1e8 N/m
k_t	Tangential contact stiffness	1e7 N/m
μ_p	Interparticle friction coefficient	0.31
c_n	Local damping coefficient	0.7

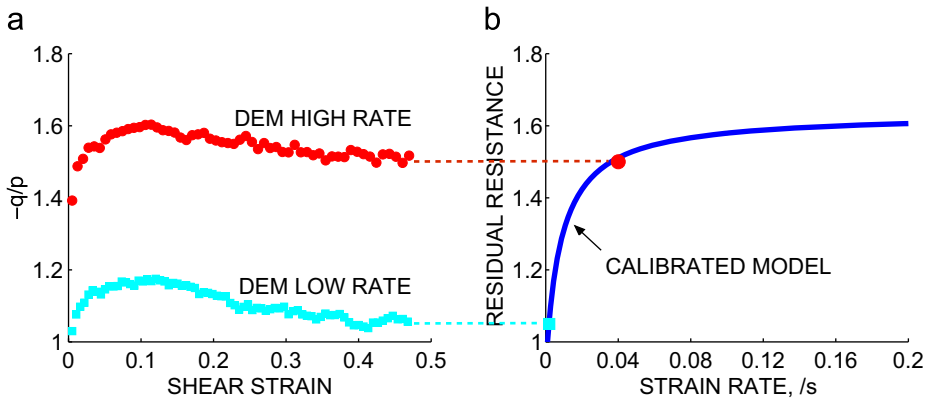

Fig. 4. Triaxial compression numerical experiments using DEM: (a) evolution of stress ratio under two different loading rates; (b) calibrated evolution of residual strength for the proposed model, cf., Eq. (2.10).

The lower and upper bound of the residual strength and the corresponding shear strain rate are determined such that the calibrated evolution as proposed in Eq. (2.10) passes the two known points given by DEM simulations. Fig. 4(b) shows the calibrated evolution of residual strength $\overline{\mu}$, as well as the two DEM data points. Parameters corresponding to this evolution are $\overline{\mu}_l = 0.9$, $\overline{\mu}_u = 1.6$, and $\dot{\epsilon}_s^* = 0.0085$.

To calibrate the dilatancy parameter β, the evolution of the volumetric strain vs. deviatoric strain curves for the two different strain rates in the DEM simulations are computed and shown in Fig. 5(a). Using Eq. (2.6), dilatancy can be computed using a simple finite difference scheme. The results are shown in Fig. 5(b), from which we obtain the maximum dilatancy $\beta^* \approx 0.2$ and the corresponding shear strain $\epsilon_s^* = 0.05$. The calibrated evolution of dilatancy (cf., Eq. (2.9)) is shown as the solid line in Fig. 5(b).

Remark 7. It can be seen from the above DEM triaxial compression numerical experiments that the volumetric strains and hence dilatancy do not seem to strongly depend on deviatoric strain rates. This is the reason why this dependence has been ignored in this work. However, in general, and as shown in Fig. 2(b), dilatancy can be a function of strain rates.

3.2. *Model verification: triaxial compression test at various loading rates*

To verify the proposed constitutive model, we implemented it in a finite element (FE) code to simulate boundary value problems. For comparison, we impose in the FE analysis the same boundary conditions as those in the DEM numerical experiments, but with a wider range of loading rates. The loading rates range from a quasi-static loading, where the residual strength of the material is given by the lower bound $\overline{\mu}_l$, up to 'very' fast loading rate, where the upper bound of the residual strength is approached at critical state.

Fig. 6(a) shows the resulting stress ratio $-q/p$ versus shear strain at different loading rates. The two dashed lines represent the lower and upper stress bounds, corresponding to quasi-static and infinitely fast loading, respectively. Solid lines are from FE simulations using the plasticity model with the parameters calibrated from before. The data from two

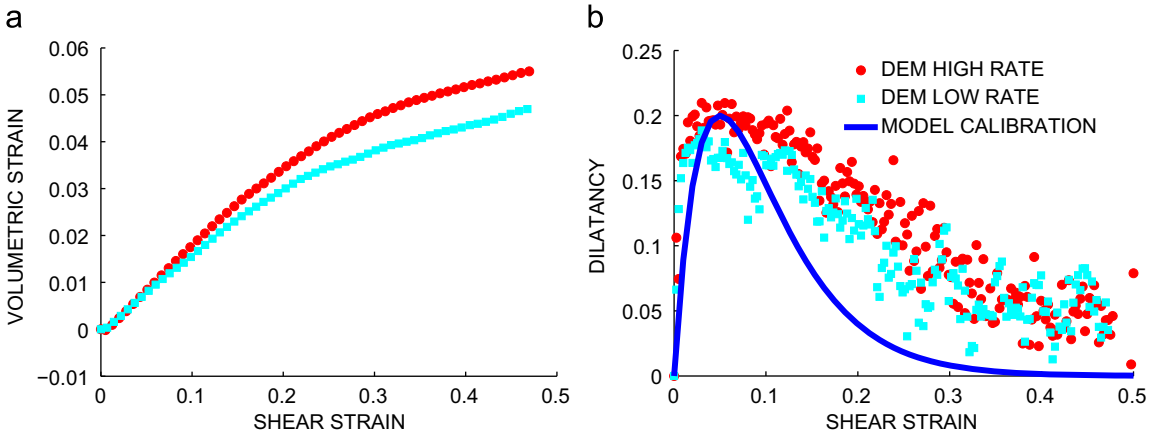

Fig. 5. Dilatancy calibration: (a) volumetric strain vs. deviatoric strain in the triaxial compression tests by DEM; (b) computed dilatancy from DEM as well as calibrated dilatancy evolution for the proposed model.

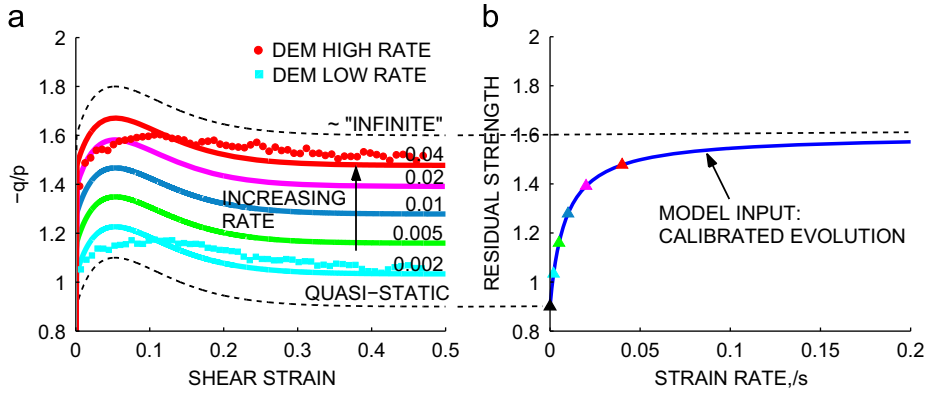

Fig. 6. (a) Stress ratio versus shear strain at different loading rate of the triaxial compression tests (numbers on the right correspond to loading rate/s); (b) Corresponding residual strength on the model calibrated evolution curve.

DEM experiments are also plotted in the same figure. The model is able to capture some key features, including the softening behavior and rate-effects. In Fig. 6(b), triangles represent the residual strengths from the FE simulation at different rates. Solid line is the model input, i.e., the calibrated evolution. It is clear that the model has correctly taken into account the rate effects on residual strength as expected.

If classical granular flow models or rate-independent plasticity models were to be used independently, the aforementioned features, such as softening and rate-effects, could not be captured. This is because the classical granular flow models usually ignores dilatancy and the material strength is given by residual resistance only, which is constant for a given strain rate. While in the rate-independent plasticity models, the rate effects on residual strength are neglected, so material strength does not evolve with loading rate. To illustrate this, we perform FE simulations neglecting either dilatancy or rate effects, respectively. Fig. 7 shows comparisons between the proposed model with (a) if dilatancy is neglected; and (b) if rate effect on residual strength is neglected. Clearly, neither simplification would yield the desired features as observed in the numerical experiments. Nevertheless, these are the current paradigms used to model granular materials.

As far as verification is concerned, the final aspect we look at is the computational efficiency. Fig. 8 shows the reported global and local residual profiles at different strain levels. It is clear to see that all iterations converge below a tolerance (in this example, 10^{-13}) within five steps. Asymptotic quadratic convergence rates are obtained for both global and local cases. This efficiency will prove crucial as the model can be implemented using explicit or implicit FE or finite difference codes and obtain solutions of boundary value problems (BVP) in seconds. This is to be contrasted with simulations using DEM, which can take up to days to run, for the same BVP.

So far, the model has been calibrated using results from numerical experiments done by discrete element simulations, and verified through some boundary value problems. In the next section, we will show two applications of the proposed model towards a classical granular flow problem and a strain localization problem in soil mechanics. These examples will further highlight the efficiency of the method and its accuracy.

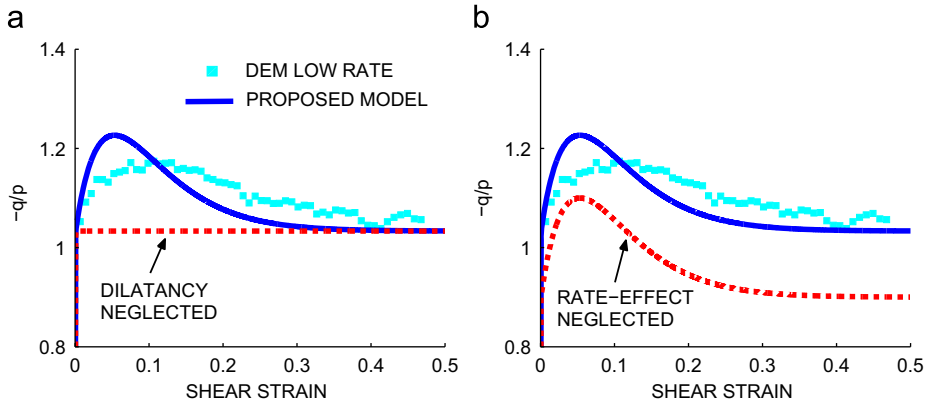

Fig. 7. Triaxial compression test at loading rate $\dot{\epsilon}_a = 0.002/s$: proposed model compared with (a) dilatancy effect neglected; (b) rate-dependence of residual strength neglected.

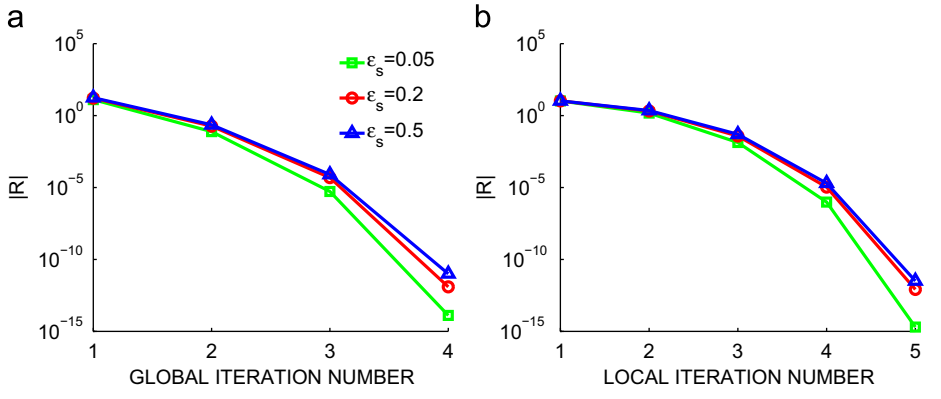

Fig. 8. Convergence profile at different strain level, for (a) global level; (b) local (material point) level. R is the residual.

4. Numerical examples: application to granular flow and classical shear banding problem

In this section, the proposed constitutive model is utilized to simulate a granular flow problem and a plane strain shear banding problem. These two examples represent classical problems studied in the physics community for understanding fluid-like behavior in granular flow, and in the soil mechanics community for understanding solid-like behavior of granular materials under quasi-static macroscopic loading. In the first example, DEM simulations are used as benchmarks to which the continuum model will be compared. The intention is to show that the simple proposed constitutive model is able to seamlessly capture the transition from solid-like to fluid-like behavior, as well as steady-state flow. In the second example, a physical plane strain compression experiment will be analyzed, showing the improved residual strength given by the proposed model. The plane strain compression example demonstrates the importance of rate effects once shear bands form within otherwise homogeneously deforming samples.

4.1. Granular flow along an inclined infinite slope

In this section, numerical experiments of granular flow along an inclined infinite slope are compared against simulations performed using the proposed model. The numerical experiments are carried out using discrete element simulations, with dimensions of the simulation box shown in Fig. 9. Periodic boundary conditions are enforced in the flow direction, as well as in the y direction so that the sidewall effects on the flow are neglected. The surface of the inclined slope is glued with one layer of particles. The granular assembly consists of monodispersed spheres with radius $r=1.2$ mm. In the numerical experiments, the simulation box is initially horizontal and the granular assembly is in a solid-like state. Then, the simulation box is instantaneously tilted to an angle θ from the horizontal direction to induce granular flow. Some (intermittent) particle movements are observed when the inclination angle $\theta=19^\circ$, but it is not until $\theta=22^\circ$ that steady-state granular flow can be achieved. If $\theta>25^\circ$, flow will keep accelerating without bound, i.e., no steady-state flow can be reached. These DEM results allow us to obtain bounds for our continuum model, as $\theta=19^\circ$ seems to correspond to the angle of repose and $\theta=25^\circ$ introduces an upper bound for the residual strength. Further, since the problem is essentially one-dimensional, only velocity profiles along the depth z direction and surface velocities are reported.

To simulate the granular flow problem using the continuum model, we have to solve the momentum balance equation written as

$$\nabla\cdot\boldsymbol{\sigma}+\rho\boldsymbol{g}=\rho\frac{\mathrm{d}\boldsymbol{v}}{\mathrm{dt}} \tag{4.1}$$

where $\boldsymbol{\sigma}$ is the Cauchy stress tensor, ρ is the particle density, $\boldsymbol{g}$ is gravitational acceleration vector and $\boldsymbol{v}$ is the velocity. Also, the boundary conditions are: traction free on the top surface, zero displacement/velocity at the bottom of the assembly. It should be noted that once sidewall effects and surface roughness are taken into account (Delannay et al., 2007; Goujon et al., 2003; Mills et al., 2000), different boundary conditions have to be chosen.

Finite difference method is implemented to solve Eq. (4.1). Time and spatial discretizations are carefully chosen such that the Courant–Friedrichs–Lewy stability criterion is satisfied (Courant et al., 1967). The proposed rate-dependent constitutive model is used to describe material behavior and the resulting finite difference governing equation reads,

$$\Delta v=\frac{1}{1+\mu\beta}\Delta t g\cos\theta(\tan\theta-\mu) \tag{4.2}$$

where v is the velocity in the flow direction at a given space finite difference node and $\Delta v=v_{n+1}-v_n$ and $\Delta t=t_{n+1}-t_n$, representing time discretization. Eq. (4.2) is the discrete version of Eq. (4.1) plus constitutive assumptions. Also, we have

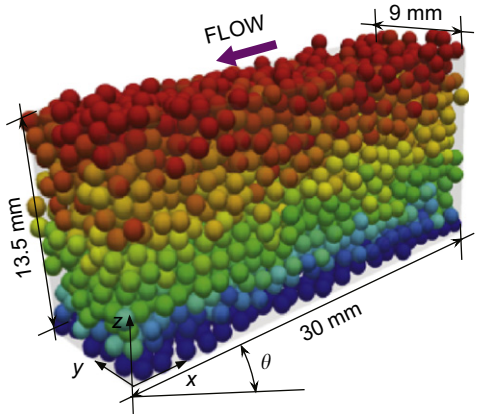

Fig. 9. Assembly of monodispersed granular particles with radius of 1.2 mm on a slope inclined at angle θ from the horizontal plane.

exploited the infinite character of the problem and hence quantities only vary in the z-direction. Also implied in Eq. (4.2) is the relationship between internal strength furnished by μ and external forces furnished by $\tan\theta$ (gravity). As long as the material can produce enough internal strength to balance external forces, equilibrium or steady state conditions will be achieved. Otherwise, the external loads will drive the system into continuous acceleration.

The frictional resistance μ is given by Eq. (2.11). Material parameters corresponding to the infinite slope problem are calibrated as follows. As noted before, the angle of repose is defined as the angle at which intermittent flow begins, which is observed form DEM simulations to be 19°, hence, $\overline{\mu}_l = \tan 19^\circ$. By the same token, continuous flow is achieved in DEM simulations at 22°. In our model, we interpret this 3° difference as a result of the peak dilation, hence, we assume $\beta^* = \tan 3^\circ$ with a corresponding (assumed) $\dot{\epsilon}_s^* = 3.5$. Finally, since the DEM simulations grow unbounded when $\theta > 25^\circ$ we assume $\overline{\mu}_l = \tan 25^\circ$.

Fig. 10 shows velocity profiles for various angle inclinations as a function of depth at selected time stations. Dots correspond to DEM simulations while solid lines are results from our continuum model. Colors represent specific time stations in the simulation. It can be seen that the velocity increases gradually, eventually reaching a steady-state profile. The continuum model is able to reproduce the velocity profiles observed in DEM well and is able to capture the transition from solid-like behavior (close to zero velocity) to fluid-like behavior, eventually resulting in steady state conditions. It should be noted that the flow layer height chosen for the DEM simulations is approximately ten particles. As described in Pouliquen and Forterre (2009), Rajchenbach (2003), Silbert et al. (2003), linear velocity profiles at steady state are typically obtained for relatively shallow flows. This is observed in this paper as well. For taller flow layers, say above 20 particles in height, steady state velocities could be nonlinear.

Surface velocity is also of particular interest. Fig. 11 shows the evolution of surface velocity for different inclination angles where steady state flows can be reached. The steady state surface flow velocity increases with inclination angles. Again, the simple proposed model is able to reproduce this key feature, and matches well with numerical DEM experiments. Also, this figure displays the clear rate dependent behavior of the material. At steady-state, and as shown in Eq. (4.2), accelerations are zero and the material strength $\mu = \tan\theta$. Hence, by looking at the steady-state velocities, one can obtain steady-state strain rates that correspond to residual strengths as shown in Fig. 11. This means that the material is increasing in strength since it is able to equilibrate at higher inclination angles, at the expense of higher steady-state velocities (higher strain rates). This feature can only be fully captured by the proposed rate-dependent continuum model.

To show the limitations of using classic modeling paradigms we perform simulations with either rate-independent plastic model and Bingham fluid model. To capture the first classical model, we simply turn off the rate dependence in the

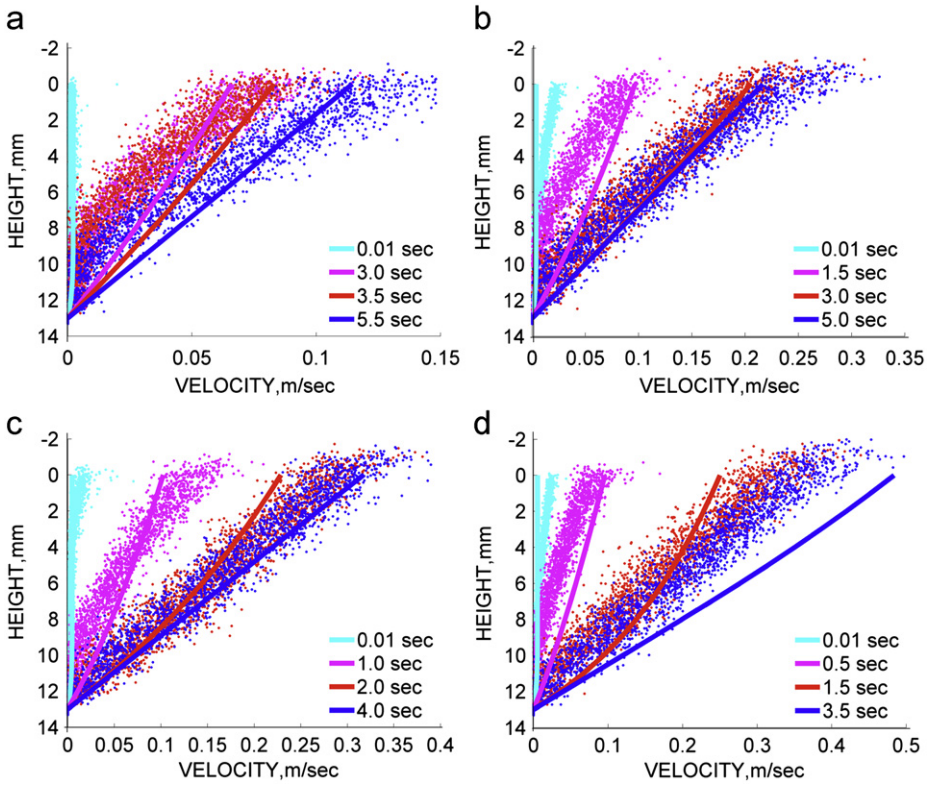

Fig. 10. Velocity (along the flow direction) profiles for different inclination angles (a) $\theta = 22^\circ$; (b) $\theta = 23^\circ$; (c) $\theta = 23.5^\circ$; (d) $\theta = 24^\circ$ (dots: numerical experiments; solid lines: model calculation).

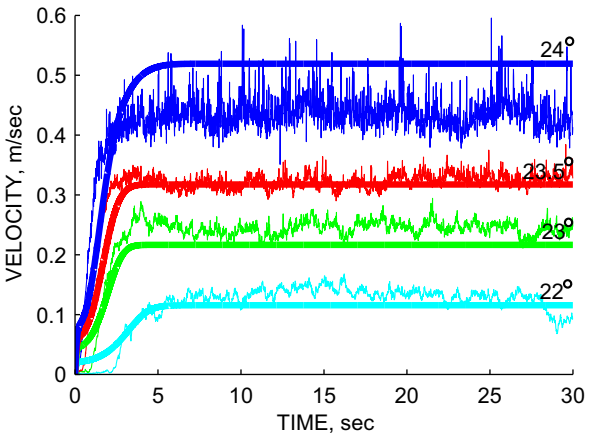

Fig. 11. Evolution of surface velocity (flow direction) for different inclination angles (nonsmooth lines: DEM numerical experiments; smooth lines: continuum model calculation).

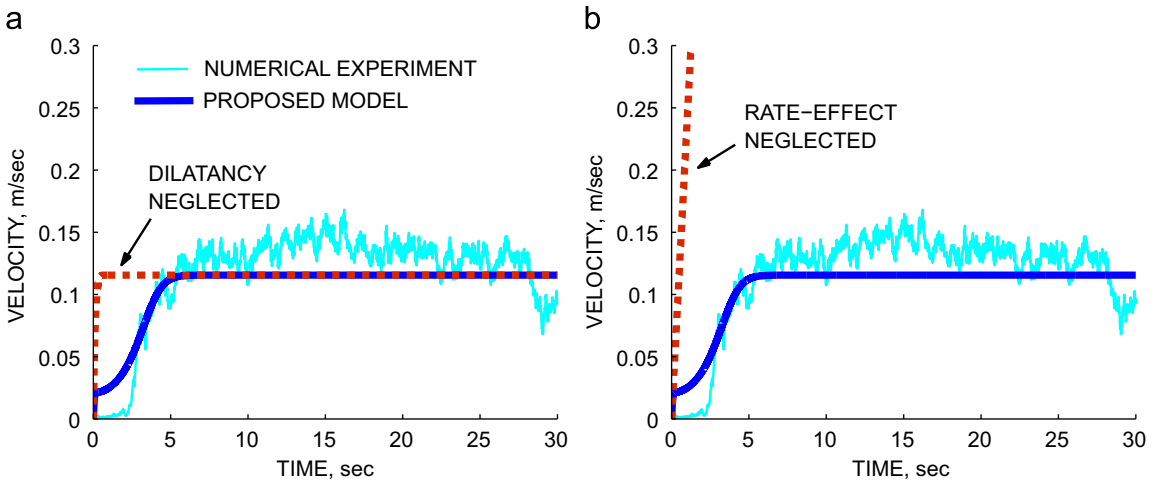

Fig. 12. Granular flow along inclined surface $\theta = 22^{\circ}$: the proposed model compared with (a) dilatancy effect neglected; (b) rate-dependence of residual strength neglected.

residual strength and make $\overline{\mu} = \tan 19^{\circ}$ constant. For the Bingham flow model, we turn off the dilatancy contribution and make $\beta = 0$. Fig. 12 shows results for inclination angle $\theta = 22^{\circ}$. If dilatancy is neglected, as shown in Fig. 12(a), the granular flow reaches steady-state almost right at the beginning. No transition from solid to fluid state is observed. If the residual strength remains constant, i.e., no rate effect, the flow will keep accelerating and never reaches steady state, as shown in Fig. 12(b). This highlights the importance of the combined model as being the only one to capture all the salient features: dilatancy dominated plasticity at early stages of deformation (solid-like regime), transition marked by full use of dilatancy, and residual strength rate dependent response (fluid-like regime) where deformations are purely isochoric.

4.2. Plane strain shear banding problem

In this section, the proposed continuum model is applied to analyze the behavior of a physical experiment on dense sand under plane strain condition. This is a revisit of the analysis done by Andrade and Tu (2009), where the rate effect on the residual strength $\overline{\mu}$ was neglected. While the previous analysis in Andrade and Tu (2009) captured the behavior of the materials well for most part of the loading, disparity between simulation and experiment at the critical state was clearly observed. It is believed that the rate-independent model may have missed some important feature of the material behavior, i.e., different strain rates inside and outside the shear band after localization. The objective of the current analysis is to show that, by adopting the proposed rate-dependent constitutive model, the effects of strain rate on material behavior is taken into account, and material residual strength could be more realistically captured.

The physical experiment was performed by Mooney et al. (1998) on a masonry sand sample of $140 \times 80 \times 40$ mm in dimensions. Plane strain was enforced by two rigid (smooth) walls, in the 80 mm direction. The sample was initially

consolidated anisotropically with axial stress $\sigma_a = -210$ kPa, and lateral stress $\sigma_r = -105$ kPa. After consolidation, the lateral stress was kept constant while the top plate was moved down with a loading rate of $\dot{\epsilon}_a \approx 1.4\%/\text{h}$. A dominant shear band inclined 63° from the horizontal axis was observed when the global axial strain reached about 3%. Evolution of dilation angle ψ was extracted using stereophotogrammetry, and was related to dilatancy parameter β through

$$\beta = \tan\psi \tag{4.3}$$

Fig. 13 shows the evolution of dilatancy angle obtained in the experiment (red circles). This phenomenological evolution of dilation will be used in this example instead of the equation proposed in (2.9). This concept of using dilation evolution from local strains has been used before in the context of multiscale simulations which details can be found in Andrade and Tu (2009), Tu et al. (2009). In Fig. 13 the solid line corresponds to the idealized evolution of dilation angle for materials inside the band, while the dotted line is for materials outside the band. The assumption of a constant dilation angle after localization outside the band is immaterial, since all plastic deformations are concentrated within the shear band and the material outside undergoes elastic unloading.

In the numerical simulations, the proposed rate-dependent constitutive model is used to describe material behavior, with the Drucker–Prager type yield surface and non-associative flow rule as presented before. The frictional resistance μ is related to dilatancy parameter β and residual resistance $\overline{\mu}$ through Eq. (2.11), and therefore depends on shear strain rate. Instead of using Eq. (2.9) for β, the measurements from the experiment shown in Fig. 13 are directly incorporated into the model. Calibrated parameters used in the model are two elastic constants $E = 40$ MPa, $\nu = 0.2$; and $\overline{\mu}_l = 1.15$, $\overline{\mu}_u = 1.5$, $\dot{\epsilon}_s^* = 1.0$.

It has been shown that the characteristic length of shear bands in granular materials is in the order of 10–20 mean particle diameters. Since most samples have characteristic macroscopic dimensions in the order of thousands of grains, strain rates inside the shear band are bound to jump by orders of magnitude once a band forms. If the material is rate-dependent, this could measurably change the behavior of the material post bifurcation. This is the idea pursued on this example. The proposed rate-dependent model is able to take into account this effect. Shown in Fig. 14 is the evolution of the residual strength inside and outside the shear band throughout the simulation. There is a significant increase of the residual strength for materials inside the shear band right at the point of localization due to the increase of strain-rate. For materials outside, the residual strength remains close to the constant value $\overline{\mu}_l = 1.15$. If a rate-independent model is used, there would be no difference in the residual strength for materials inside and outside the band.

The evolution of the global stress ratio with global axial strain is shown in Fig. 15. There is some disparity between the rate-independent model and experiment results, especially post bifurcation and at critical state. As mentioned before, it is hypothesized that the significantly higher strain rate, could trigger rate effects inside the shear band. In this particular case, there is a slight increase in strength, which seems to improve the results significantly, as shown by the solid line in Fig. 15. Similarly, if a simulation is conducted using only a rate-dependent fluid model (by turning off the dilatancy effect), the model completely misses the transient effect and produces a constant stress ratio corresponding to the final residual strength in the continuum model. This is clearly undesirable. The continuum model proposed here is able to obtain better results than the classic counterparts. Also, in Fig. 15 we have reported the results of the rate-dependent model using a finer mesh. It can be seen that the results are relatively mesh-independent, with the stress ratio values for both fine and coarse meshes following almost identical trends.

Finally, the deviatoric stress and strain contours of the sample at the end of the simulation are shown in Figs. 16 and 17. There are clear concentrations of shear stress and strain inside the band as expected. Also, it can be seen that the shear strain contours are virtually the same for the rate-independent and rate-dependent models, as expected. On the other hand, because rate-dependence of material strength is taken into account, the proposed rate-dependent model displays higher shear stresses inside the band. This of course, results in an apparent increase in global sample strength.

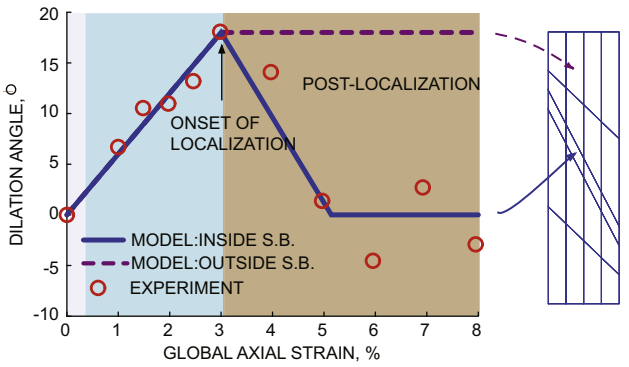

Fig. 13. Evolution of dilation angle observed in the experiment and input into the finite element model.

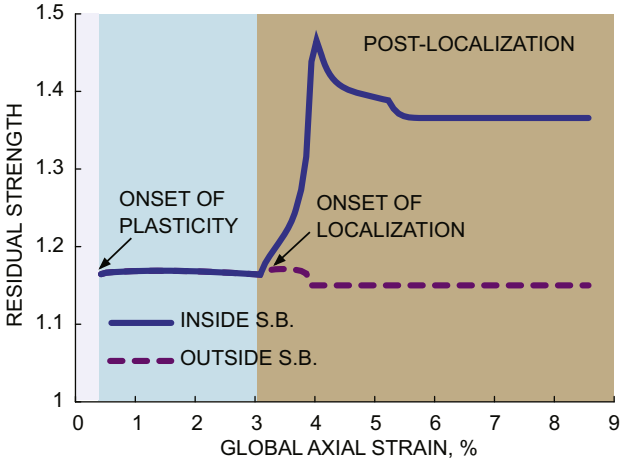

Fig. 14. Evolution of the residual strength $\overline{\mu}$ inside and outside the shear band.

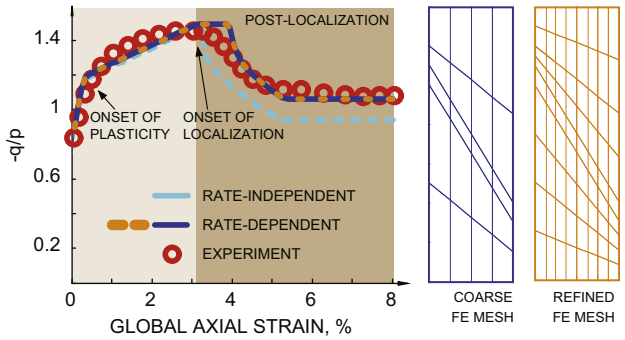

Fig. 15. Evolution of stress ratio with global axial strain. Results are shown for two different meshes, clearly indicating relatively mesh-independent results.

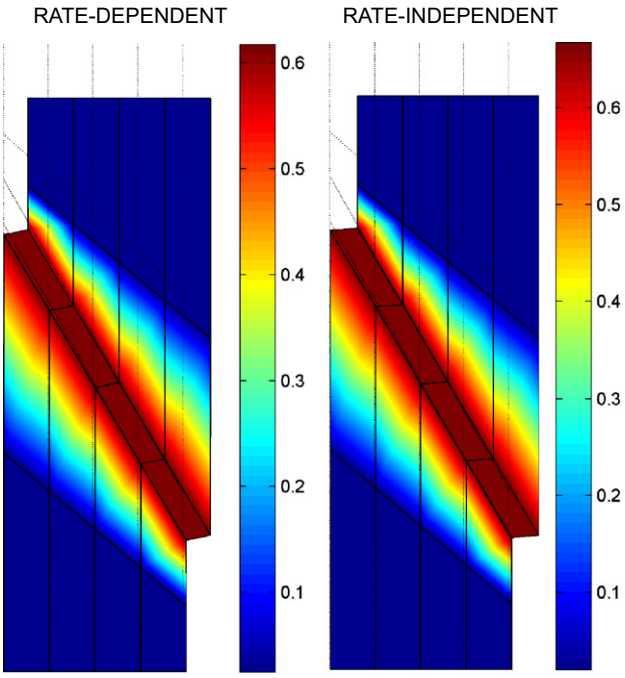

Fig. 16. Shear strain contour at the end of the simulation ($\epsilon_a \approx 8.5\%$) for both rate-dependent and rate-independent models.

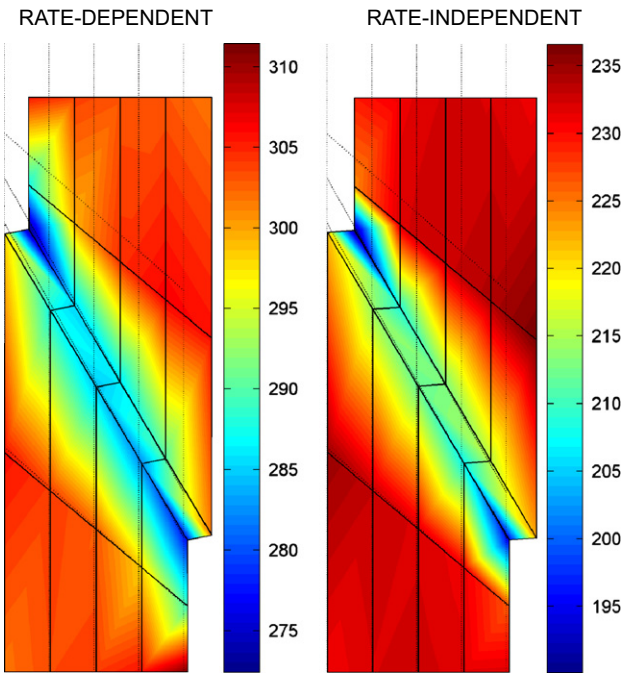

Fig. 17. Shear stress contour at the end of the simulation ($\epsilon_a \approx 8.5\%$) for both rate-dependent and rate-independent models.

5. Conclusions

We have presented a rate-dependent plasticity model for dilative granular media aiming to bridge the solid- and fluid-like state of such materials. The model emanates from classical plasticity in soil mechanics where material strength is composed of a dilatancy strength and a residual resistance. The model accommodates the material behavior transition by proposing the evolution of dilatancy, which plays a key role in the solid-like state but vanishes towards the fluid-like state. The residual strength is proposed to be rate-dependent, affording it key features of fluid-like state in granular materials. The model is calibrated using numerical experiments by discrete element method simulations and verified by boundary value problems. Though simple in form, the capability of the model to reconcile classical plasticity and rheology camps has been shown through the successful application to a classical granular flow problem, where key features such as solid–fluid transition, velocity profiles and free-surface velocity evolutions are captured. Neither classical rate-independent plasticity theory nor steady-state granular flow model alone would be able to capture these features at the same time. Finally, the model is applied to a shear banding problem, where the rate-effect on material strength inside and outside shear band has been considered and results from the model match well with experiment observations. It is anticipated that the proposed model will spur the development of more accurate models able to transit classic plasticity and non-Newtonian fluid models, and as a result capture the observed physics with higher accuracy.

Acknowledgments

Support for this work is provided by AFOSR Grant number FA9550-08-1-1092. This support is gratefully acknowledged.

References

Andrade, J.E., Borja, R.I., 2006. Capturing strain localization in dense sands with random density. Int. J. Numer. Methods Eng. 67, 1531–1564.
Andrade, J.E., Ellison, K.C., 2008. Evaluation of a predictive constitutive model for sands. J. Geotech. Geoenviron. Eng. 134, 1825–1828.
Andrade, J.E., Tu, X., 2009. Multiscale framework for behavior prediction in granular media. Mech. Mater. 41 (6), 652–669.
Berton, G., Delannay, R., Richard, P., Taberlet, N., Valance, A., 2003. Two-dimensional inclined chute flows: transverse motion and segregation. Phys. Rev. E 68, 051303.
Borja, R.I., Sama, K.M., Sanz, P.F., 2003. On the numerical integration of three-invariant elastoplastic constitutive models. Comput. Methods Appl. Mech. Eng. 192, 1227–1258.
Brown, E., Forman, N.A., Orellana, C.S., Zhang, H., Maynor, B., Betts, D.E., DeSimone, J.M., Jaeger, H.M., 2010. Generality of shear thickening in dense suspensions. Nat. Mater. 9, 220–224.
Courant, R., Friedrichs, K., Lewy, H., 1967. On the partial difference equations of mathematical physics. IBM J. Res. Dev. 11, 215–234.
Cundall, P.A., 2001. A discontinuous future for numerical modelling in geomechanics? Geotech Eng. ICE 149, 41–47.
Cundall, P.A., Strack, O.D.L., 1979. A discrete numerical model for granular assemblies. Géotechnique 29, 47–65.

da Cruz, F., Emam, S., Prochnow, M., Roux, J.-N., Chevoir, F., 2005. Photophysics of dense granular materials: discrete simulation of plane shear flows. Phys. Rev. E 72, 021309.
Delannay, R., Louge, M., Richard, P., Taberlet, N., Valance, A., 2007. Towards a theoretical picture of dense granular flows down inclines. Nat. Mater. 6, 99–108.
Desai, C.S., Siriwardane, H.J., 1984. Constitutive Laws for Engineering Materials. Prentice-Hall, Inc.
du Pont, S.C., Fischer, R., Gondret, P., Perrin, B., Rabaud, M., 2005. Instantaneous velocity profiles during granular avalanches. Phys. Rev. Lett. 94, 048003.
Fall, A., Huang, N., Bertrand, F., Ovarlez, G., Bonn, D., 2008. Shear thickening of constarch suspensions as a reentrant jamming transition. Phys. Rev. Lett. 100, 018301.
Forterre, Y., Pouliquen, O., 2008. Flows of dense granular media. Annu. Rev. Fluid Mech. 40, 1–24.
Fung, Y.C., 1977. A First Course in Continuum Mechanics. Prentice-Hall, Inc., Englewood Cliffs, NJ.
GDR MiDi, 2004. On dense granular flows. Eur. Phys. J. E 14, 341–365.
Goujon, C., Thomas, N., Dalloz-Dubrujeaud, B., 2003. Monodisperse dry granular flows on inclined planes: role of roughness. Eur. Phys. J. E 11, 147–157.
Greve, R., Koch, T., Hutter, K., 1994. Unconfined flow of granular avalanches along a partly curved surface: experiments and theoretical predictions. Proc. Math. Phys. Sci. 445, 415–435.
Jaeger, H.M., Nagel, S.R., Behringer, R.P., 1996. Granular solids, liquids, and gases. Rev. Mod. Phys. 68, 1259–1273.
Jop, P., Forterre, Y., Pouliquen, O., 2005. Crucial role of side walls for granular surface flows: consequences for the rheology. J. Fluid Mech. 541, 167–192.
Jop, P., Forterre, Y., Pouliquen, O., 2006. A constitutive law for dense granular flows. Nature 441, 727–730.
Jop, P., Forterre, Y., Pouliquen, O., 2007. Initiation of granular surface flows in a narrow channel. Phys. Fluids 19, 088102.
Lois, G., Lemaitre, A., Carlson, J.M., 2005. Numerical tests of constitutive laws for dense granular flows. Phys. Rev. E 72, 051303.
Manzari, M.T., Dafalias, Y.F., 1997. A critical state two-surface plasticity model for sands. Géotechnique 43, 255–272.
Mills, P., Loggia, D., Tixier, M., 1999. Model for a stationary dense granular flow along an inclined wall. Europhys. Lett. 45, 733.
Mills, P., Tixier, M., Loggia, D., 2000. Influence of roughness and dilatancy for dense granular flow along an inclined wall. Eur. Phys. J. E 1, 5–8.
Mooney, M.A., Finno, R.J., Viggiani, M.G., 1998. A unique critical state for sand? J Geotech. Geoenviron. Eng. 124, 1100–1108.
Orpe, A.V., Khakhar, D.V., 2004. Solid–fluid transition in a granular shear flow. Phys. Rev. Lett. 93, 068001.
Pailha, M., Pouliquen, O., 2009. A two-phase flow description of the initiation of underwater granular avalanches. J. Fluid Mech. 633, 115–135.
Pestana, J.M., Whittle, A.J., 1999. Formulation of a unified constitutive model for clays and sands. Int. J. Numer. Anal. Methods Geomech. 23, 1215–1243.
Pouliquen, O., Forterre, Y., 2009. A non-local rheology for dense granular flows. Philos. Trans. R. Soc. 367, 5091–5107.
Pouliquen, O., Cassar, C., Jop, P., Forterre, Y., Nicolas, M., 2006. Flow of dense granular material: towards simple constitutive laws. J. Stat. Mech. Theory Exp., P07020.
Rajchenbach, J., 2003. Dense, rapid flows of inelastic grains under gravity. Phys. Rev. Lett. 90, 144302.
Rajchenbach, J., 1990. Flow in powders: from discrete avalanches to continuous regime. Phys. Rev. Lett. 65, 2221–2224.
Reynolds, O., 1885. On the dilatancy of media composed of rigid particles in contact. Philos. Mag. J. Sci. 20, 468–481.
Rowe, P.W., 1962. The stress–dilatancy relation for static equilibrium of an assembly of particles in contact. Proc. R. Soc. London A 269, 500–527.
Savage, S.B., Hutter, K., 1989. The motion of a finite mass of granular material down a rough incline. J. Fluid Mech. 199, 177–215.
Schofield, A., Wroth, P., 1968. Critical State Soil Mechanics. McGraw-Hill, New York.
Silbert, L.E., Ertas, D., Grest, G.S., Halsey, T.C., Levine, D., Plimpton, S.J., 2001. Granular flow down an inclined plane: Bagnold scaling and rheology. Phys. Rev. E 64, 051302.
Silbert, L.E., Landry, J.W., Grest, G.S., 2003. Granular flow down a rough inclined plane: transition between thin and thick piles. Phys. Fluids 15, 1.
Simo, J.C., Hughes, T.J.R., 1998. Computational Inelasticity. Prentice-Hall, New York.
Stroud, M.A., 1971. The Behavior of Sand at Low Stress Levels in the Simple Shear Apparatus. Ph.D. Thesis. Cambridge University, Cambridge, UK.
Taylor, D.W., 1948. Fundamentals of Soil Mechanics. John Wiley & Sons Ltd, New York.
Thompson, P.A., Grest, G.S., 1991. Granular flow: friction and dilatancy transition. Phys. Rev. Lett. 67, 1751–1754.
Tu, X., Andrade, J.E., Chen, Q., 2009. Return mapping for nonsmooth and multiscale elastoplasticity. Comput. Methods Appl. Mech. Eng. 198, 2286–2296.
Wieland, M., Gray, J.M.N.T., Hutter, K., 1999. Channelized free-surface flow of cohesionless granular avalanches in a chute with shallow lateral curvature. J. Fluid Mech. 392, 73–100.
Wood, D.M., 1990. Soil Behaviour and Critical State Soil Mechanics. Cambridge University Press, Cambridge, UK.
Zhang, Y., Campbell, C.S., 1992. The interface between fluid-like and solid-like behavior in two-dimensional granular flows. J. Fluid Mech. 237, 541–568.